

Journal of Materials Chemistry A

Accepted Manuscript



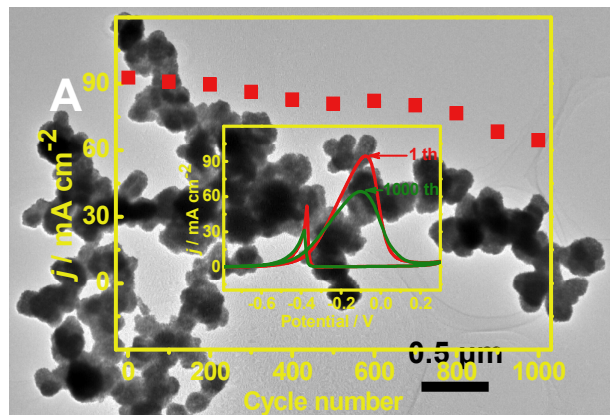
This is an *Accepted Manuscript*, which has been through the Royal Society of Chemistry peer review process and has been accepted for publication.

Accepted Manuscripts are published online shortly after acceptance, before technical editing, formatting and proof reading. Using this free service, authors can make their results available to the community, in citable form, before we publish the edited article. We will replace this *Accepted Manuscript* with the edited and formatted *Advance Article* as soon as it is available.

You can find more information about *Accepted Manuscripts* in the [Information for Authors](#).

Please note that technical editing may introduce minor changes to the text and/or graphics, which may alter content. The journal's standard [Terms & Conditions](#) and the [Ethical guidelines](#) still apply. In no event shall the Royal Society of Chemistry be held responsible for any errors or omissions in this *Accepted Manuscript* or any consequences arising from the use of any information it contains.

Graphical Abstract



A simple and facile one-pot polyol method was developed for synthesis of porous Pd₆₃Ag₃₇ alloy coral-like nanostructures, which exhibited the improved electrocatalytic activity and enhanced stability for glycerol oxidation reaction.

Simple polyol synthesis of porous coral-like palladium-silver alloy nanostructures with enhanced electrocatalytic activity for glycerol oxidation reaction

Pei Song, Jiu-Ju Feng, Fei-Ying Guo, Ai-Jun Wang*

College of Chemistry and Life Science, College of Geography and Environmental Science, Zhejiang Normal University, Jinhua, 321004, China

**Corresponding author: ajwang@zjnu.cn (A. J. Wang), Tel./Fax: +86 579 82282269.*

Abstract

In this work, porous bimetallic palladium-silver (Pd₆₃Ag₃₇) alloy nanocorals were synthesized by a simple and facile one-pot polyol method. The composition and morphology of the nanocrystals were well controlled by changing the concentrations of the precursors. The obtained nanocrystals were mainly characterized by scanning electron microscopy, transmission electron microscopy, X-ray diffraction, X-ray photoelectron spectra, and Brunauer-Emmett-Teller method. Porous Pd₆₃Ag₃₇ nanocorals had the enlarged electrochemically active surface area (55.85 m² g⁻¹), and exhibited the enhanced electrocatalytic activity and improved stability for glycerol oxidation reaction as compared to commercial Pd black, owing to the unique porous coral-like nanostructures and synergistic interactions of the alloyed bimetals.

Keywords: Polyol synthesis; bimetallic alloy; Nanocorals; Porous structure; Glycerol oxidation reaction

1. Introduction

Many efforts have been devoted to direct liquid fuel cells (DLFCs), which are considered to be one of the promising clean energy sources with high energy conversion efficiency and lower environmental pollution.¹⁻³ To date, lots of liquid anodic fuels have been employed, such as methanol,⁴ ethanol,⁵ formic acid,⁶ ethylene glycol,⁷ and glycerol.⁸

Among them, glycerol attracts more interest in recent years, due to its lower toxicity, renewability from biomass, and relatively high theoretical energy density as compared to other alcohol fuels.^{9,10} However, each carbon carries an alcohol group in glycerol and consequently it tends to be partially oxidized to mesoxalate without C-C bond breaking and CO_3^{2-} production, causing 10 electrons exchanged, rather than 14 electrons for the complete oxidation to CO_3^{2-} .^{11,12}

Pt-based nanomaterials are widely used as electrocatalysts in fuel cells, because they possess high catalytic activity among the anode catalysts for electro-oxidation of small organic fuels and the cathode catalysts for oxygen reduction.^{13,14} However, the high cost and serious CO self-poisoning of Pt severely limit its potential applications in fuel cells.¹⁵

Recent extensive researches focus on the development of non-platinum electrocatalysts with comparable catalytic properties. Fortunately, Pd is considered as the promising alternative candidates for both the anode and cathode catalysis in DLFCs, because of its comparable catalytic properties but much lower cost relative to Pt.^{15,16}

Moreover, introducing transition metals (e.g., Au, Ag, Cu, and Ni) into Pd is highly desired both for improving the catalytic activity of Pd and cutting down the cost. For example, Ma et al. found that carbon supported Pd₃₀Au₇₀ nanoparticles with significantly low Pd content showed remarkably higher activity than commercial Pt/C and Pd/C.¹⁷ In another example, Chen and his coworkers prepared PdAg alloy nanowires with enhanced catalytic activity as compared to commercial Pd/C.²

Besides the alloying of transition metals, fabricating Pd-based nanocatalysts with different structures and/or morphology are also a powerful way to enhance their catalytic activity and stability. Up to now, various Pd and Pd-based nanomaterials have been synthesized as potential nanocatalysts, including porous Pd rods,¹⁸ branched Pd dendrites,¹⁹ PdAg flowers,²⁰ and hollow NiPdAu/C particles.²¹

Notably, three dimensional porous structures contribute to the remarkably improved stability, owing to the enlarged surface area-to-volume ratio and more active sites available for absorbed molecules.²²⁻²⁴ The branched Pd nanodendrites displayed substantially enhanced catalytic activity for oxygen reduction and ethanol oxidation as compared with commercial Pd/C.¹⁹ The flower-like porous PdAg nanocrystals exhibited improved catalytic activity and better stability for ethanol oxidation.²⁰

The polyol synthesis provides a simple and versatile approach to prepare nanomaterials.^{25,26} This is attributed to the ability for polyol to dissolve many metallic precursor salts, temperature-dependent reducing power, and relatively high boiling point (e.g., ethylene glycol of ~196 °C).^{27, 28} In addition, the reductant can be

continuously *in situ* produced upon heating the polyol. Thus, the changes in the kinetics of nanostructure growth can be negligible as the reductant is added or consumed.

In this work, porous Pd₆₃Ag₃₇ alloy nanocorals were prepared by a simple one-pot polyol method, and their electrocatalytic properties were examined using glycerol oxidation reaction (GOR) as a bench model system.

2. Experimental section

2.1 Chemicals and materials

Palladium(II) trifluoroacetate ((CF₃COO)₂Pd, 98%), silver trifluoroacetate (CF₃COOAg, 98%), poly(vinylpyrrolidone) (PVP, M_w ≈ 58,000), ethylene glycol (EG), glycerol, and commercial Pd black were all obtained from Aladdin Chemistry Co. Ltd (Shanghai, China). All the other chemicals were of analytical grade and used without further purification. All the aqueous solutions were prepared with twice-distilled water in the whole experiments.

2.2 Preparation of highly porous Pd₆₃Ag₃₇ alloy nanocorals

For typical synthesis of highly porous Pd₆₃Ag₃₇ alloy nanocorals, 200 mg of PVP and 9.0 mL of EG were added into a round-bottomed flask and heated in an oil bath at 160 °C under magnetic stirring, followed by the quick injection of another 1.0 mL of EG solution containing 33.3 mg of (CF₃COO)₂Pd and 11.1 mg of CF₃COOAg (the molar ratio is 2:1) with a pipette. The reaction solution was maintained at 160 °C for 3

h and then cooled down to room temperature in air. The resulting black precipitates were collected by centrifugation and thoroughly washed with ethanol and water for several times, and dried in vacuum at 60 °C for further characterization. EDS analysis confirms the coexistence of Pd and Ag with the atomic ratio (Pd to Ag) of 63:37 (Fig. S1A, Electronic supplementary information, ESI). Thus, the products denoted as Pd₆₃Ag₃₇.

For comparison, control samples were prepared with (CF₃COO)₂Pd and CF₃COOAg with the molar ratio of 1:1 and 1:2, respectively. The coexistences of Pd and Ag with the atomic ratio (Pd to Ag) of the compositions were 50:50 and 40:60, respectively (Fig. S1B and C, ESI). They denoted as Pd₅₀Ag₅₀ and Pd₄₀Ag₆₀, respectively.

2.3 Characterizations

The morphology and crystal structure of the samples were determined by scanning electron microscopy (SEM, LEO-1530), transmission electron microscopy (TEM), and high resolution TEM (HR-TEM) on a JEM-2100F transmission electron microscope operating at an acceleration voltage of 200 kV equipped with selective area electron diffraction (SAED) and energy dispersive X-ray spectrometer (EDS). The elemental mappings were recorded on a scanning transmission electron microscope (STEM) with a high-angle annular dark-field (HAADF) detector (HITACHI S-5500). The specific surface area of the sample was measured by Brunauer-Emmett-Teller (BET) method on a Surface Area Analyzer (NOVA2000-09,

USA) at 77.3 K through N₂ adsorption. X-ray diffraction (XRD) analysis was performed at a Philips PW3040/60 diffractometer with Cu K α radiation source ($\lambda = 0.15418$ nm). X-ray photoelectron spectra (XPS) were acquired to determine the chemical surface properties on a K-Alpha XPS spectrometer (SCIENTIFIC ESCALAB 250) with Al K α X-ray radiation (1486.6 eV) for excitation.

2.4 Electrochemical measurements

All the electrochemical measurements were carried out at room temperature on a CHI 660D electrochemical workstation (CHI Instruments, Chenhua Co., Shanghai, China) with a three-electrode cell, containing a bare or modified glassy carbon electrode (GCE, 3 mm in diameter) as the working electrode, a platinum wire as the counter electrode, and a saturated calomel electrode (SCE) as the reference electrode.

For typical preparation of Pd₆₃Ag₃₇ nanocorals modified electrode, 2 mg of the samples were dispersed into 2 mL of water and ultrasonicated to form a dark homogeneous suspension. Subsequently, 6 μ L (0.006 mg) of the suspension was uniformly casted on the GCE and dried in air, followed by the deposition of 4 μ L of Nafion (0.05 wt. %) to tightly combine the deposit on the electrode surface. For comparison, Pd₅₀Ag₅₀, Pd₄₀Ag₆₀, and commercial Pd black modified electrode was prepared in a similar way.

The electrochemically active surface area (ECSA) of the catalyst was determined by CO-stripping voltammograms. Specifically, the catalyst surface was first saturated with CO by bubbling CO through 0.5 M H₂SO₄ at 0.1 V for 30 min. The remaining

CO in the solution was purged with N₂ for another 30 min. Then, the CO-stripping voltammograms were recorded in 0.5 M H₂SO₄ (pH = 0.38) at the scan rate of 50 mV s⁻¹. The ECSA of the catalyst was calculated by the following equation:²⁹

$$\text{ECSA} = \frac{Q_{(\text{CO})}}{m_{(\text{Pd})} \times 420}$$

where $Q_{(\text{CO})}$ is the charges of CO desorption-electrooxidation (μC), $m_{(\text{Pd})}$ is the weight of Pd loading on the electrode surface (μg), and 420 is the charge required to oxidize a monolayer of CO on the catalyst ($\mu\text{C cm}^{-2}$).

The cyclic voltammetry experiments were carried out in 1.0 M KOH containing 0.5 M glycerol at a scan rate of 50 mV s⁻¹, and the chronoamperometry experiments were conducted in 1.0 M KOH containing 0.5 M glycerol at -0.2 V. All the experiments were performed at room temperature, if not stated otherwise.

3. Results and discussion

3.1 Characterizations

The morphology and structural features of the as-synthesized products were characterized by TEM and HR-TEM measurements. As shown in Fig. 1A, well-defined coral-like Pd₆₃Ag₃₇ alloy nanostructures are observed through the polyol synthetic synthesis, which consist of many branched nanocorals. High magnification TEM image further reveals that the branch-like corals are composed of numerous small and irregular nanoparticles which are interconnected to generate abundant pores (Fig. 1B). Furthermore, HRTEM images taken from the marked sections (Fig. 1B) clearly display well-resolved lattice fringes (Fig. 1C and D), with the interplanar

spacing distance of 0.228 nm corresponding to the (111) planes of Pd₆₃Ag₃₇ alloy. The value is smaller than that of the (111) crystal planes of the face-centered cubic (fcc) Ag (0.236 nm, JCPDS-04-0783), but larger than that of the fcc Pd (0.225 nm, JCPDS-46-1043), showing the formation of Pd₆₃Ag₃₇ alloy again. These observations are matched well with Pd₆₃Ag₃₇ nanocatalysts in the literature.^{4, 30} In addition, their polycrystalline nature is strongly demonstrated by the corresponding SAED pattern (inset in Fig. 1B). Moreover, the morphology of the samples (i.e., Pd₅₀Ag₅₀ and Pd₄₀Ag₆₀) remarkably change by tuning the molar ratios of the precursors (CF₃COO)₂Pd/CF₃COOAg, as displayed in Fig. S2 (ESI). For the sample of Pd₅₀Ag₅₀ procured from the molar ratio of 1:1 (Fig. S2A, ESI), small coral-like fragments are obtained, while there are only thin nanochains observed for Pd₄₀Ag₆₀ sample with the molar ratio of 1:2 (Fig. S2B, ESI). It reveals that the molar ratio of the precursors plays an important role in the formation of the nanocorals.

SEM and BET measurement were conducted to characterize the surface structure of Pd₆₃Ag₃₇ nanocorals. As illustrated in Fig. 2A, the sample exhibits rough surfaces, which are distributed with numerous pores. Besides, the nitrogen adsorption-desorption isotherm curves measured at 77.35 K exhibit an evident hysteresis loop at a relative pressure P/P_0 ranging from 0.6 to 1.0 (Fig. 2B). Accordingly, the dominating pore-size distribution is located in the range of 3-13 nm (inset in Fig. 2B), as calculated by the Barrett-Joyner-Halenda method.³⁰ The BET surface area is 17.21 m² g⁻¹ for Pd₆₃Ag₃₇ nanocorals, as well as the pore volume of 0.04 cm³ g⁻¹ and the average pore size of 10.84 nm. The porous structure would

endow Pd₆₃Ag₃₇ nanocorals with the enlarged ECSA and offer more active sites available for glycerol oxidation.

Element analysis was conducted to clarify the distribution of Pd and Ag in Pd₆₃Ag₃₇ nanocorals. Fig. 3A-C show the selected-area element analysis mapping images of Pd, Ag and the overlap, in which Pd and Ag are uniformly dispersed in the entire nanocorals, reflecting the formation of homogeneous Pd₆₃Ag₃₇ alloyed structure,³¹ as supported by the EDS line scanning profiles (Fig. 3D).

XRD analysis was employed to check the crystal structure of Pd₆₃Ag₃₇ nanocorals (Fig. 4). In the XRD pattern of Pd₆₃Ag₃₇ nanocorals, there are four diffraction peaks emerged at 39.34°, 45.50°, 66.61°, and 80.04°, which are well assigned to the (111), (200), (220), and (311) planes of Pd₆₃Ag₃₇ alloy.³² For comparison, bulk Pd (JCPDS: 46-1043) and Ag (JCPDS: 04-0783) are also provided. All the diffraction peaks for Pd₆₃Ag₃₇ nanocorals coincidentally show up between the diffraction peaks from bulk Pd and Ag, which further demonstrate the alloyed structure of Pd₆₃Ag₃₇ nanocorals. More importantly, the diffraction peaks from Pd₆₃Ag₃₇ nanocorals shift to lower 2θ values as compared with bulk Pd, suggesting the increase of lattice constant by alloying with Ag.^{32,33} This observation is in good accordance with Pd₆₃Ag₃₇ alloy nanospheres in the previous report.⁵

XPS measurements were performed to determine the surface composition and oxidation states of Pd₆₃Ag₃₇ nanocorals. Fig. 5A shows the survey XPS spectrum, which reveals that the sample is mainly composed of C, O, Ag, and Pd elements. It can be seen that the high-resolution XPS spectrum of Pd 3d can be deconvoluted into

two doublets at around 334.84, 335.55, 340.10, and 340.81 eV (Fig. 5B), indicating metallic Pd and PdO present in the nanocatalyst.^{29, 31} Further detailed analysis shows that the percentage of Pd (0) is 65.91%, indicating that the Pd precursor was efficiently reduced to metallic Pd. Furthermore, the binding energies of Pd are negatively shifted compared with those of commercial Pd black (Fig. S3, ESI). The negative shift of Pd 3d peaks is possibly due to the doped Ag facilitating the electron transfer with Pd (electronegativity: Pd = 2.20, Ag = 1.93).

Similarly, Ag 3d_{5/2} and 3d_{3/2} peaks are located at 368.25 and 374.28 eV in the high-resolution XPS spectrum of Ag 3d (Fig. 5C), respectively.^{34, 35} It means that Ag mainly present in the zero valent state in Pd₆₃Ag₃₇ nanocorals.

3.2 Formation mechanism

Fig. 6 shows the formation mechanism of porous coral-like Pd₆₃Ag₃₇ alloy nanostructures based on the fast nucleation and attachment growth.^{4, 6, 36} Firstly, large numbers of Pd and Ag atoms are generated immediately after the addition of the precursors, owing to the extremely fast reduction rate of the polyol synthesis method. As the concentrations of Pd and Ag atoms have reached hyper-saturated states, Pd and Ag nanoclusters are formed via the homogeneous nucleation. Next, the primary Pd and Ag nanoclusters would aggregate to form larger particles to minimize the total surface free energy of the system with the assistance of PVP as a structure director.³⁶ As a result, coral-like Pd₆₃Ag₃₇ nanostructures are formed eventually.

3.3 Electrochemical measurements

The ECSA of Pd₆₃Ag₃₇ nanocorals, Pd₅₀Ag₅₀, Pd₄₀Ag₆₀ and commercial Pd black modified electrodes were analyzed by CO-stripping measurements in 0.5 M H₂SO₄ (Fig. 7). According to the CO-stripping voltammograms of Pd₆₃Ag₃₇ nanocorals (Fig. 7A) Pd₅₀Ag₅₀ (Fig. 7B), Pd₄₀Ag₆₀ (Fig. 7C) and commercial Pd black (Fig. 7D) modified electrodes, the ECSA of Pd₆₃Ag₃₇ nanocorals modified electrode is calculated to be 55.85 m² g⁻¹, which is larger than Pd₅₀Ag₅₀ (35.52 m² g⁻¹), Pd₄₀Ag₆₀ (32.79 m² g⁻¹), and commercial Pd black (7.11 m² g⁻¹) modified electrodes. The enlarged ECSA of Pd₆₃Ag₃₇ nanocorals is ascribed to the large electrochemically accessible surface and interface area because of the unique porous structures as demonstrated by TEM and SEM characterizations.^{37, 38}

Moreover, Fig. 7 show that the onset potentials of CO oxidation on Pd₆₃Ag₃₇ nanocorals, Pd₅₀Ag₅₀ and Pd₄₀Ag₆₀ modified electrodes (ca. 0.71 V, 0.68 V and 0.66 V) are more negative than that on commercial Pd black modified electrode (ca. 0.75 V), which means that the doping of Ag promotes the removal of CO from the surface of PdAg alloy.^{39, 40} These results indicate the enhanced catalytic activity of PdAg alloy.³⁹

Cyclic voltammetry measurements were used to evaluate the electrocatalytic properties of Pd₆₃Ag₃₇ nanocorals for GOR, using Pd₅₀Ag₅₀, Pd₄₀Ag₆₀ and commercial Pd black as referenced materials (Fig. 8A). As shown in Fig. 8A, the forward oxidation peak current of glycerol on Pd₆₃Ag₃₇ nanocorals modified electrode reaches the maximum value of 94.45 mA cm⁻², which is about 2.89, 4.99, and 8.78 folds larger than Pd₅₀Ag₅₀, Pd₄₀Ag₆₀ and commercial Pd black modified electrodes (32.62,

18.96 and 10.78 mA cm⁻²).

It is well known that the specific activity (normalized to the ECSA) and the mass activity (normalized to the mass of metal (Pd) loading) of a catalyst can effectively evaluate the intrinsic activity.⁴¹ Fig. 8B shows the ECSA-normalized and mass-normalized maximum catalytic currents of Pd₆₃Ag₃₇ nanocorals, Pd₅₀Ag₅₀, Pd₄₀Ag₆₀ and commercial Pd black modified electrodes. The specific activity of Pd₆₃Ag₃₇ nanocorals modified electrode is 6.07 mA cm⁻², which is larger than Pd₅₀Ag₅₀ (1.08 mA cm⁻²), Pd₄₀Ag₆₀ (6.07 mA cm⁻²) and commercial Pd black (4.67 mA cm⁻²) modified electrodes. According to the comparison of mass activity in Fig. 8B, Pd₆₃Ag₃₇ nanocorals, Pd₅₀Ag₅₀ and Pd₄₀Ag₆₀ modified electrodes all have larger values (1603.19, 773.08, and 565.87 mA mg⁻¹ Pd) than commercial Pd black (150.48 mA mg⁻¹ Pd), indicating that alloying Ag with Pd significantly enhances the oxidation activity of glycerol. Moreover, the oxidation peak current density of Pd₆₃Ag₃₇ nanocorals is higher than the other catalysts in the literature.^{12, 42} These results show that Pd₆₃Ag₃₇ nanocorals have improved electrocatalytic performance for GOR.

The catalytic activity and long-term stability of Pd₆₃Ag₃₇ nanocorals modified electrode for GOR were evaluated by chronoamperometry at an applied potential of -0.2 V (curve a, Fig. 9A), using Pd₅₀Ag₅₀ (curve b, Fig. 9A), Pd₄₀Ag₆₀ (curve c, Fig. 9A) and commercial Pd black (curve d, Fig. 9A) modified electrodes as the contrast. As shown in Fig. 9A, the two catalysts show the high initial oxidation current densities, which are come from the double-layer charging and numerous available active sites on the catalyst surface.⁵ Afterwards, the currents drop down sharply,

implying the formation of intermediate carbonaceous species such as CO-like species which poison the active sites. During the whole reaction process, the currents on Pd₆₃Ag₃₇ nanocorals modified electrode are much higher and decrease more slowly as compared to those on Pd₅₀Ag₅₀, Pd₄₀Ag₆₀ and commercial Pd black modified electrodes. These observations confirm that Pd₆₃Ag₃₇ nanocorals modified electrode has much higher catalytic activity and better stability for GOR, as further demonstrated by cyclic voltammetry curves (Fig. 9B) where the catalytic current density is almost constant (only reduced by 3.35%) within 200 cycles. Furthermore, after scanning for 1000 cycles, the peak current density still maintain 69.47% of the initial value (inset in Fig. 9B). The enhanced stability is attributed to the presence of Ag in Pd₆₃Ag₃₇ alloy. As known, OH⁻ ions are more easily adsorbed onto Pd₆₃Ag₃₇ alloy instead of monometallic Pd, which will accelerate the oxidation of the produced intermediates (such as glyceraldehydes, glycerate, and tartronate etc.) and release more active sites on the surface of Pd₆₃Ag₃₇ nanocorals.^{5, 40, 43} The foregoing explain is also supported by the result that Pd₅₀Ag₅₀ and Pd₄₀Ag₆₀ modified electrodes exhibit an improved stability as compared to commercial Pd black. The detailed schematic illustration for GOR on Pd₆₃Ag₃₇ nanocatalyst is provided in Fig. S4 (ESI).

Pd₆₃Ag₃₇ nanocorals exhibit the enhanced catalytic activity and improved stability for GOR as compared to commercial Pd black, which may be ascribed to the following reasons. Firstly, Pd₆₃Ag₃₇ nanocorals own much larger electrochemically accessible surface area, offering more active sites for GOR because of their unique porous coral-like nanostructure. As demonstrated, Pd₆₃Ag₃₇

nanocorals modified electrode exhibit higher anodic peak current ($1603.2 \text{ mA mg}^{-1} \text{ Pd}$) than $\text{Pd}_{65}\text{Ag}_{35}/\text{C}$ nanoparticles ($629.6 \text{ mA mg}^{-1} \text{ Pd}$),⁴ which indicate that the larger surface area to volume ratio may play an essential role to the enhancement of the performance. Secondly, alloying Pd with Ag can promote glycerol oxidation by changing the electronic property of Pd. It is known that the adsorption ability of the adsorbate onto alloys is intimately correlated with the d-band center of the metals.⁴⁴ After alloying Pd with Ag, the d-band center of Pd is shifted positively in $\text{Pd}_{63}\text{Ag}_{37}$ nanocorals, showing the stronger adsorption ability and increased binding energy of the adsorbate, which promotes alcohol oxidation on the metallic alloy surface, as also strongly supported by the density functional calculations.^{45, 46} As a result, it is facilitated that glycerol oxidation on the surface of $\text{Pd}_{63}\text{Ag}_{37}$ nanocorals.

4. Conclusions

In summary, $\text{Pd}_{63}\text{Ag}_{37}$ alloy nanocatalysts with porous coral-like structure were synthesized by a simple and facile polyol method. The composition and morphology of the nanocrystals, well-controlled by changing the molar ratios of the precursors, had great effects on the electrocatalytic activity. The electrochemical measurements exhibited the improved catalytic activity and enhanced stability of $\text{Pd}_{63}\text{Ag}_{37}$ nanocorals for GOR, which is attributed to the enlarged specific surface area, unique porous morphology and alloyed structure. This work not only provides a facile route for preparation of porous bimetallic alloy nanostructure, but also provides a kind of novel anodic catalyst with enhanced catalytic performance for liquid fuel cells.

Acknowledgement

This work was financially supported by National Natural Science Foundation of China (Nos. 21475118, 21175118 and 21275130).

References

1. B. C. H. Steele and A. Heinzl, *Nature*, 2001, **414**, 345-352.
2. Y. Lu and W. Chen, *ACS Catalysis*, 2012, **2**, 84-90.
3. E. H. Yu, X. Wang, U. Krewer, L. Li and K. Scott, *Energy Environ. Sci.*, 2012, **5**, 5668-5680.
4. Z. Yin, Y. Zhang, K. Chen, J. Li, W. Li, P. Tang, H. Zhao, Q. Zhu, X. Bao and D. Ma, *Sci. Rep.*, 2014, **4**, 4288.
5. C. Peng, Y. Hu, M. Liu and Y. Zheng, *J. Power Sources*, 2015, **278**, 69-75.
6. Y. Wang, S.-I. Choi, X. Zhao, S. Xie, H.-C. Peng, M. Chi, C. Z. Huang and Y. Xia, *Adv. Funct. Mater.*, 2014, **24**, 131-139.
7. J.-J. Feng, D.-L. Zhou, H.-X. Xi, J.-R. Chen and A.-J. Wang, *Nanoscale*, 2013, **5**, 6754-6757.
8. S. Carrettin, P. McMorn, P. Johnston, K. Griffin, C. J. Kiely and G. J. Hutchings, *Phys. Chem. Chem. Phys.*, 2003, **5**, 1329-1336.
9. H. J. Kim, S. M. Choi, S. Green, G. A. Tompsett, S. H. Lee, G. W. Huber and W. B. Kim, *Appl. Catal. B: Environ.*, 2011, **101**, 366-375.
10. J.-h. Zhang, Y.-j. Liang, N. Li, Z.-y. Li, C.-w. Xu and S. P. Jiang, *Electrochim.*

- Acta*, 2012, **59**, 156-159.
11. A. Ilie, M. Simoes, S. Baranton, C. Coutanceau and S. Martemianov, *J. Power Sources*, 2011, **196**, 4965-4971.
 12. M. Simões, S. Baranton and C. Coutanceau, *Appl. Catal. B: Environ.*, 2010, **93**, 354-362.
 13. A. Chen and P. Holt-Hindle, *Chem. Rev.*, 2010, **110**, 3767-3804.
 14. D. Chen, X. Zhao, S. Chen, H. Li, X. Fu, Q. Wu, S. Li, Y. Li, B.-L. Su and R. S. Ruoff, *Carbon*, 2014, **68**, 755-762.
 15. C. Bianchini and P. K. Shen, *Chem. Rev.*, 2009, **109**, 4183-4206.
 16. S.-S. Li, Y.-Y. Hu, J.-J. Feng, Z.-Y. Lv, J.-R. Chen and A.-J. Wang, *Int. J. Hydrogen Energy*, 2014, **39**, 3730-3738.
 17. Z. Yin, M. Chi, Q. Zhu, D. Ma, J. Sun and X. Bao, *J. Mater. Chem. A*, 2013, **1**, 9157-9163.
 18. X. Wang, W. Wang, Z. Qi, C. Zhao, H. Ji and Z. Zhang, *J. Power Sources*, 2010, **195**, 6740-6747.
 19. Q. Gao, M.-R. Gao, J.-W. Liu, M.-Y. Chen, C.-H. Cui, H.-H. Li and S.-H. Yu, *Nanoscale*, 2013, **5**, 3202-3207.
 20. W. Hong, J. Wang and E. Wang, *Electrochem. Commun.*, 2014, **40**, 63-66.
 21. C. Shang, W. Hong, J. Wang and E. Wang, *J. Power Sources*, 2015, **285**, 12-15.
 22. Z. Yin, H. Zheng, D. Ma and X. Bao, *J. Phys. Chem. C*, 2009, **113**, 1001-1005.
 23. W. Hong, Y. Fang, J. Wang and E. Wang, *J. Power Sources*, 2014, **248**, 553-559.
 24. C. M. A. Parlett, K. Wilson and A. F. Lee, *Chem. Soc. Rev.*, 2013, **42**, 3876-3893.

25. J. Chen, T. Herricks and Y. Xia, *Angew. Chem. Int. Ed.*, 2005, **44**, 2589-2592.
26. Y. Xiong, J. Chen, B. Wiley, Y. Xia, S. Aloni and Y. Yin, *J. Am. Chem. Soc.*, 2005, **127**, 7332-7333.
27. M. H. Kim, B. Lim, E. P. Lee and Y. Xia, *J. Mater. Chem.*, 2008, **18**, 4069-4073.
28. C. Ducamp-Sanguesa, R. Herrera-Urbina and M. Figlarz, *J. Solid State Chem.*, 1992, **100**, 272-280.
29. C. Hu, Z. Bai, L. Yang, J. Lv, K. Wang, Y. Guo, Y. Cao and J. Zhou, *Electrochim. Acta*, 2010, **55**, 6036-6041.
30. L.-X. Chen, J.-N. Zheng, A.-J. Wang, L.-J. Wu, J.-R. Chen and J.-J. Feng, *Analyst*, 2015, **140**, 3183-3192.
31. Q. Zhang, X. Guo, Z. Liang, J. Zeng, J. Yang and S. Liao, *Nano Research*, 2013, **6**, 571-580.
32. G. Li, L. Jiang, Q. Jiang, S. Wang and G. Sun, *Electrochim. Acta*, 2011, **56**, 7703-7711.
33. C. Xu, Y. Liu, J. Wang, H. Geng and H. Qiu, *J. Power Sources*, 2012, **199**, 124-131.
34. M. Liu, Y. Lu and W. Chen, *Adv. Funct. Mater.*, 2013, **23**, 1289-1296.
35. Y. Ma, J. Bansmann, T. Diemant and R. J. Behm, *Surf. Sci.*, 2009, **603**, 1046-1054.
36. J.-J. Lv, J.-N. Zheng, S.-S. Li, L.-L. Chen, A.-J. Wang and J.-J. Feng, *J. Mater. Chem. A*, 2014, **2**, 4384-4390.
37. Y. Xu, R. Xu, J. Cui, Y. Liu and B. Zhang, *Chem. Commun.*, 2012, **48**, 3881-3883.

38. G. Fu, Z. Liu, Y. Chen, J. Lin, Y. Tang and T. Lu, *Nano Research*, 2014, **7**, 1205-1214.
39. Y. Wang, Z. M. Sheng, H. Yang, S. P. Jiang and C. M. Li, *Int. J. Hydrogen Energy*, 2010, **35**, 10087-10093.
40. Y. Holade, C. Morais, K. Servat, T. W. Napporn and K. B. Kokoh, *ACS Catalysis*, 2013, **3**, 2403-2411.
41. X.-Y. Liu, Y. Zhang, M.-X. Gong, Y.-W. Tang, T.-H. Lu, Y. Chen and J.-M. Lee, *J. Mater. Chem. A*, 2014, **2**, 13840-13844.
42. M. Mougenot, A. Caillard, M. Simoes, S. Baranton, C. Coutanceau and P. Brault, *Appl. Catal. B: Environ.*, 2011, **107**, 372-379.
43. S. T. Nguyen, H. M. Law, H. T. Nguyen, N. Kristian, S. Wang, S. H. Chan and X. Wang, *Appl. Catal. B: Environ.*, 2009, **91**, 507-515.
44. Z. Cui, M. Yang and F. J. DiSalvo, *ACS Nano*, 2014, **8**, 6106-6113.
45. A. Ruban, B. Hammer, P. Stoltze, H. L. Skriver and J. K. Nørskov, *J. Mol. Catal. A: Chem.*, 1997, **115**, 421-429.
46. J. Greeley, J. K. Nørskov and M. Mavrikakis, *Annu. Rev. Phys. Chem.*, 2002, **53**, 319-348.

Captions

Fig. 1 (A-B) TEM and (C) HRTEM images of Pd₆₃Ag₃₇ nanocorals. Inset in B shows the corresponding SAED pattern.

Fig. 2 (A) SEM image and (B) nitrogen adsorption/desorption analysis of Pd₆₃Ag₃₇ nanocorals. Inset shows the corresponding pore size distribution.

Fig. 3 (A-C) HAADF-STEM-EDS elemental mapping images of Pd₆₃Ag₃₇ nanocorals. (D) Cross-sectional compositional line profiles taken from Pd₆₃Ag₃₇ nanocorals. Inset shows the associated HAADF-STEM image.

Fig. 4 XRD patterns of Pd₆₃Ag₃₇ nanocorals. For comparison, bulk Pd (JCPDS: 46-1043) and Ag (JCPDS: 04-0783) are also included.

Fig. 5 Survey (A), high-resolution Pd 3d (B), and Ag 3d (C) XPS spectra of Pd₆₃Ag₃₇ nanocorals.

Fig. 6 Schematic diagram of the formation process of Pd₆₃Ag₃₇ nanocorals.

Fig. 7 CO-stripping voltammograms of Pd₆₃Ag₃₇ nanocorals (A), Pd₅₀Ag₅₀ (B), Pd₄₀Ag₆₀ (C) and commercial Pd black (D) modified electrodes in 0.5 M H₂SO₄ at a

scan rate of 50 mV s^{-1} .

Fig. 8 (A) Cyclic voltammograms of $\text{Pd}_{63}\text{Ag}_{37}$ nanocorals (curve a), $\text{Pd}_{50}\text{Ag}_{50}$ (curve b), $\text{Pd}_{40}\text{Ag}_{60}$ (curve c) and commercial Pd black (curve d) modified electrodes in 1.0 M KOH containing 0.5 M glycerol at a scan rate of 50 mV s^{-1} . (B) Comparison of the corresponding specific activity and mass activity.

Fig. 9 (A) Chronoamperometric curves of $\text{Pd}_{63}\text{Ag}_{37}$ nanocorals (curve a), $\text{Pd}_{50}\text{Ag}_{50}$ (curve b), $\text{Pd}_{40}\text{Ag}_{60}$ (curve c) and commercial Pd black (curve d) modified electrodes at -0.2 V in 1.0 M KOH containing 0.5 M glycerol. (B) Forward peak current density (j) as a function of potential scanning cycles of the $\text{Pd}_{63}\text{Ag}_{37}$ nanocorals modified electrode in 1.0 M KOH containing 0.5 M glycerol. Inset shows the corresponding cyclic voltammograms of 1th and 1000th cycles.

Figures

Fig. 1

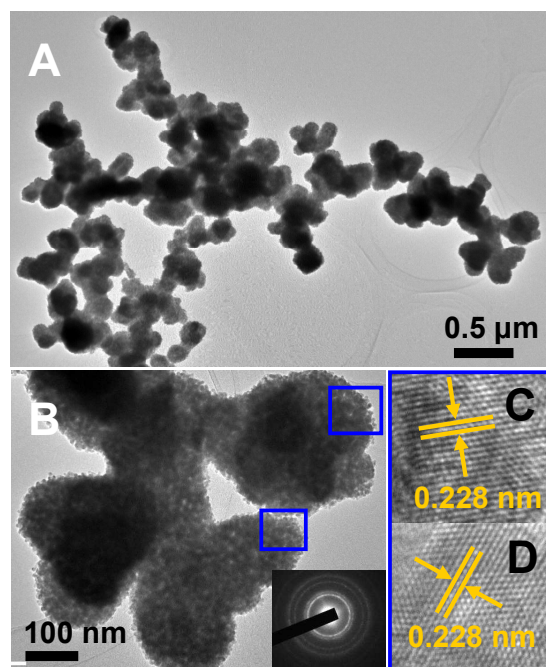


Fig. 2

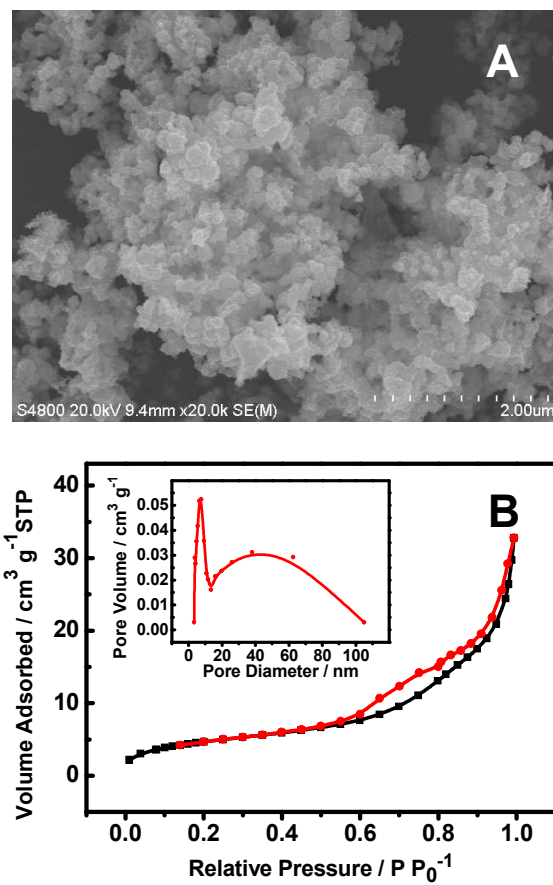


Fig. 3

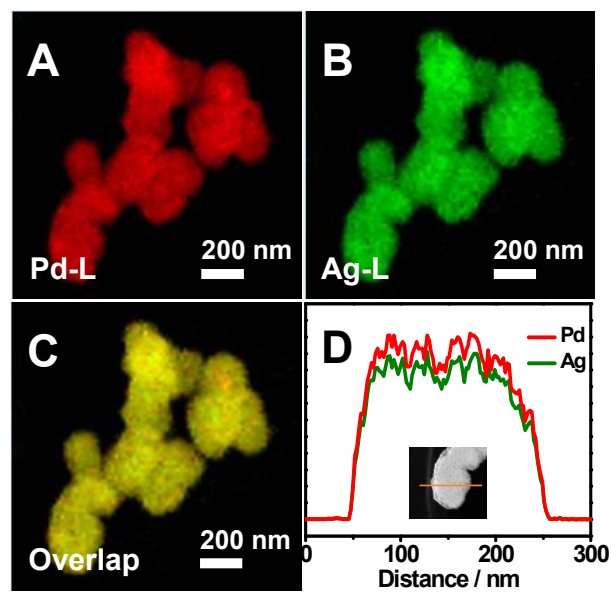


Fig. 4

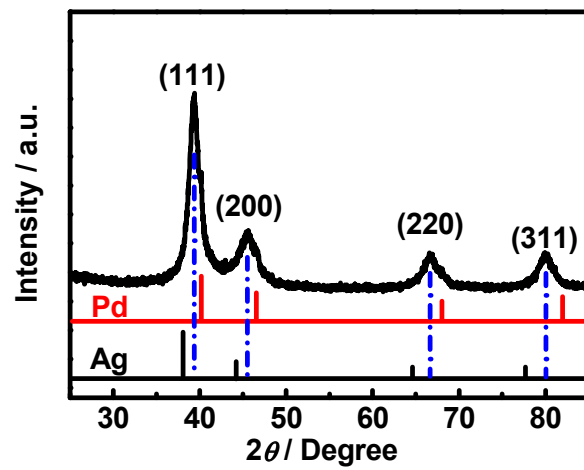


Fig. 5

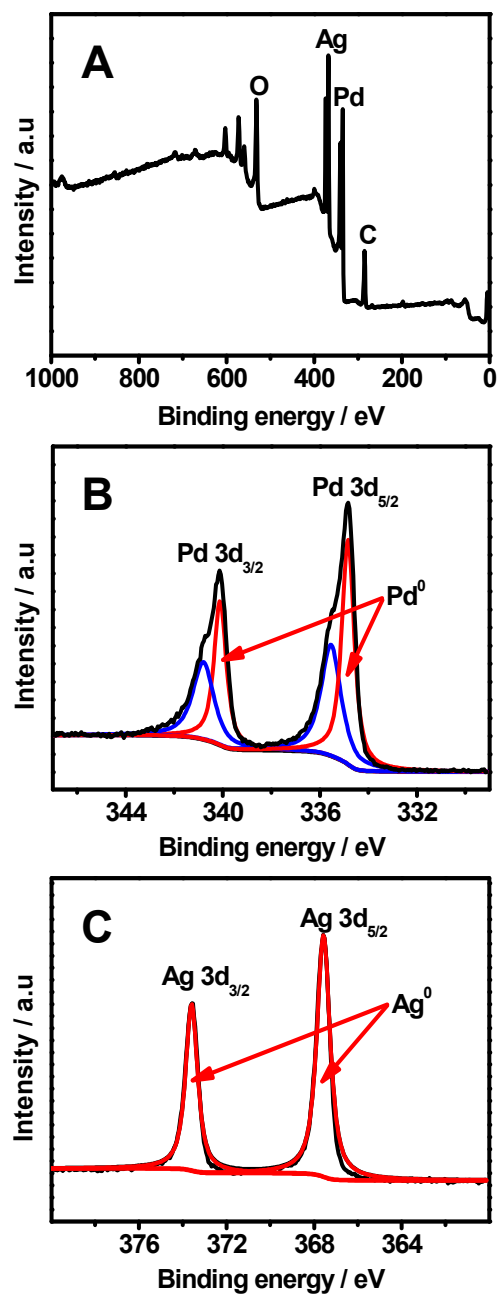


Fig. 6

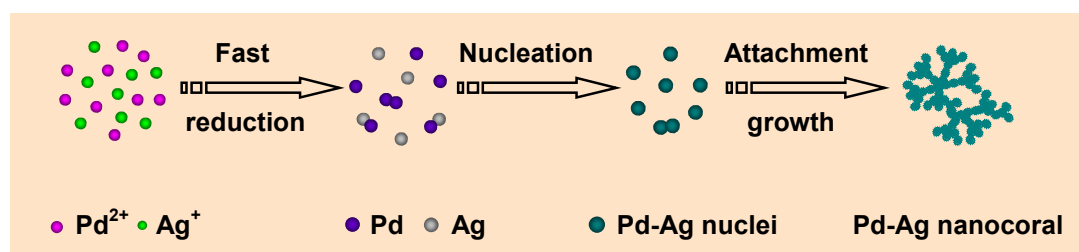


Fig. 7

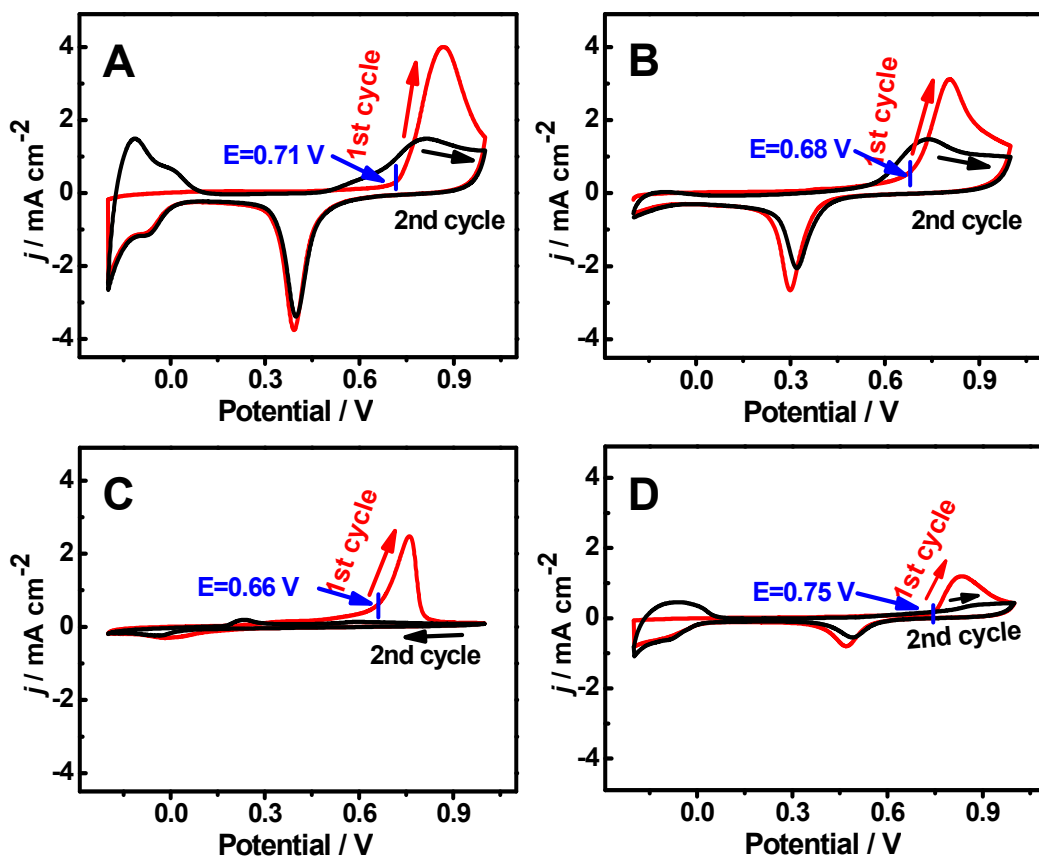


Fig. 8

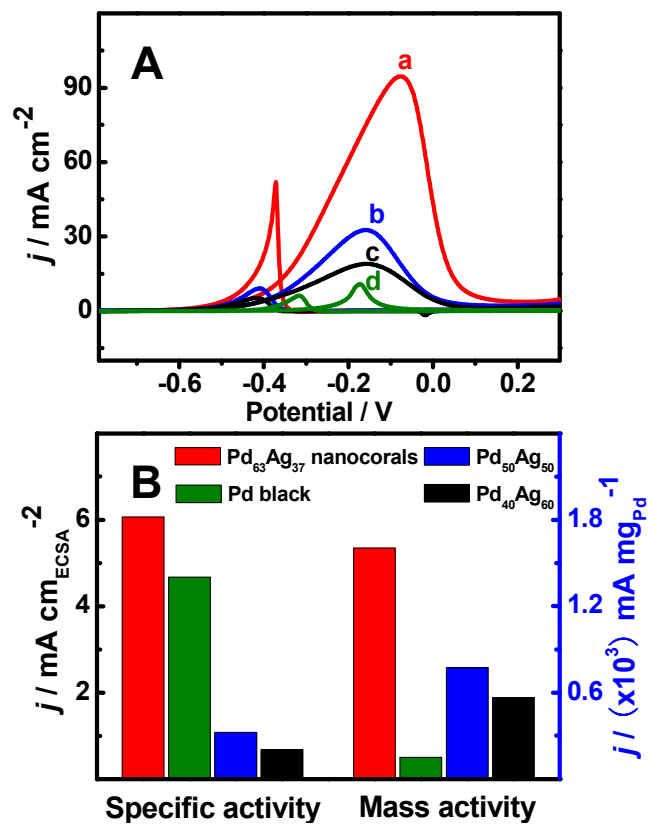


Fig. 9

